Radial anisotropy in the crust of SE Tibet and SW China from ambient noise interferometry

Hui Huang,[1] Huajian Yao,[1,2] and Robert D. van der Hilst[1]

Received 4 August 2010; revised 21 September 2010; accepted 27 September 2010; published 11 November 2010.

[1] We use Rayleigh and Love wave Green's functions estimated from ambient seismic noise to study crustal structure and radial anisotropy in the tectonically complex and seismically active region west of the Sichuan Basin and around the Eastern Himalaya Syntaxis. In agreement with previous studies, low velocity zones are ubiquitous in the mid-lower crust, with substantial variations both laterally and vertically. Discrepancies between 3-D shear velocity from either Rayleigh (V_{SV}) or Love (V_{SH}) waves are examined both in view of non-uniqueness of tomographic solutions and radial anisotropy. Low shear wave speed and radial anisotropy with $V_{SH} > V_{SV}$ are most prominent in mid-lower crust in area northwest to the Lijiang-Muli fault and around the Red River and Xiaojiang faults. This anisotropy could be caused by sub-horizontal mica fabric and its association with low velocity zones suggests mica alignment due to flow in deep crustal zones of relatively low mechanical strength. **Citation:** Huang, H., H. Yao, and R. D. van der Hilst (2010), Radial anisotropy in the crust of SE Tibet and SW China from ambient noise interferometry, *Geophys. Res. Lett.*, *37*, L21310, doi:10.1029/2010GL044981.

1. Introduction

[2] Despite decades of research, the mechanism of crustal deformation and eastward expansion of the Tibetan Plateau are still under debate. As the conjunction between the Tibetan Plateau and the Yangtze Indo-China blocks and the southern end of the trans-China seismicity belt, SE Tibet is of particular interest. GPS data [*Zhang et al.*, 2004; *Shen et al.*, 2005] and geological studies [*Wang et al.*, 1999; *Wang and Burchfiel*, 2000] show that in this region the upper crust rotates clockwise around the Eastern Himalayan Syntaxis. But how this surface motion is related to deformation at larger depth is not yet known.

[3] Along with geological data, including constraints on shortening and uplift history, the topography of this region – in particular, the gentle slope from ~5 km on the Plateau to less than 1 km in the southeast and the steep margin west of the Sichuan Basin – was used by *Royden et al.* [1997] to argue for flow in the deep crust. The area is intersected, however, by major fault systems, such as the Red River, Lijiang-Muli, Xianshuihe-Xiaojiang, and Longmenshan faults (Figure 1), which seismicity and GPS measurements [*Shen et al.*, 2005] indicate are active block boundaries. These observations mostly pertain to the (near) surface, and more direct information about the deeper crust is needed to understand the large scale deformation this region.

[4] On the one hand, recent discoveries of low velocity zones (LVZs) in middle and lower crust [*Xu et al.*, 2007; *Yao et al.*, 2008, 2010; *Li et al.*, 2009], high Poisson's ratio [*Hu et al.*, 2005; *Xu et al.*, 2007], high heat flow [*Hu et al.*, 2000], and low electrical resistivity [*Bai et al.*, 2010] suggest that at least locally the deep crust is mechanically weak. Furthermore, the change in pattern of azimuth anisotropy from upper crust to upper mantle [*Yao et al.*, 2010] suggests that the crust and mantle deform differently. These inferences are qualitatively consistent with ductile flow in the deep crust [*Royden et al.*, 1997, 2008]. On the other hand, the edges of some LVZs seem to coincide with faults [*Yao et al.*, 2008, 2010] where GPS data reveal large slip rates [*Shen et al.*, 2005]. Combined, these observations suggest that the tectonic evolution and deformation of SE Tibet is influenced by the juxtaposition of crustal blocks with or without weak zones, separated by major faults [*Yao et al.*, 2010].

[5] Radial anisotropy, that is, the difference in propagation speed of horizontally and vertically polarized waves – inferred, respectively, from Love and Rayleigh wave data – has been used to diagnose specific styles of crustal deformation [*Shapiro et al.*, 2004; *Moschetti et al.*, 2010]. For example, crustal flow can produce a horizontal mica fabric, which, in turn, can produce significant radial anisotropy [e.g., *Weiss et al.*, 1999; *Shapiro et al.*, 2004]. Following our work on crustal heterogeneity and azimuthal anisotropy in the southeastern margin of Tibet [*Yao et al.*, 2008, 2010], we determine radial anisotropy from ambient noise tomography [e.g., *Shapiro et al.*, 2005; *Yao et al.*, 2006] with empirical Green's functions (EGFs) for short- and intermediate period Rayleigh and Love wave propagation. A major objective of this study is to establish spatial correlations between LVZs and the type and strength of radial anisotropy.

2. Data and Method

[6] It is now well established that cross correlation of ambient noise recorded at two seismic stations can be used to measure the Green's function, hereinafter referred to as the empirical Green's function (EGF), of wave propagation between these stations (see auxiliary material, Section 1) [*Lobkis and Weaver*, 2001; *Weaver and Lobkis*, 2004; *Roux et al.*, 2005].[1] For our study in SE Tibet we estimate Rayleigh wave EGFs from vertical component and Love wave EGFs (Figures S1a and S1b) from transverse component data recorded in 2003 and 2004 at a temporary array of

[1]Department of Earth, Atmospheric, and Planetary Sciences, Massachusetts Institute of Technology, Cambridge, Massachusetts, USA.
[2]Now at Institute of Geophysics and Planetary Physics, Scripps Institute of Oceanography, University of California, San Diego, La Jolla, California, USA.

Copyright 2010 by the American Geophysical Union.
0094-8276/10/2010GL044981

[1]Auxiliary materials are available in the HTML. doi:10.1029/2010GL044981.

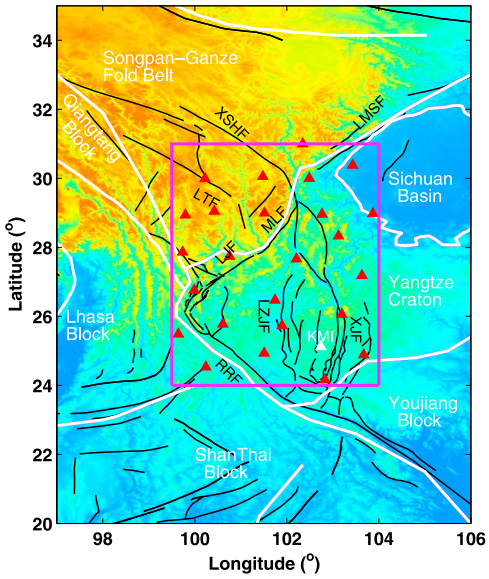

Figure 1. Location of the temporary broad-band array in Sichuan and Yunnan provinces of SW China (red triangles) and a permanent station KMI (white triangle) in Kunming, Yunnan. Black lines depict major faults [after *Wang et al.*, 1999; *Wang and Burchfiel*, 2000; *Shen et al.*, 2005] and white lines delineate tectonic boundaries. Magenta box shows the area of our study. Abbreviations: XSHF, Xianshuihe fault; LMSF, Longmenshan fault; LTF, Litang fault; LJF, Lijiang fault; MLF, Muli fault; LZJF, Luzhijiang fault; XJF, Xiaojiang fault; RRF, Red River fault.

25 stations in SE Tibet and at KMI (Kunming, Yunnan), a permanent station of the global seismograph network (Figure 1).

[7] Following *Yao et al.* [2006, 2008] we use a 3-step procedure to invert for 3-D shear wave velocity variations. In the first step, we measure phase velocity dispersion curves for appropriate station pairs (Figures S1c and S1d). In the second step, we use these dispersion curves to construct phase velocity maps at different periods (7–40s); for each point on a 0.5°-by-0.5° grid, phase velocities are then calculated for a range of frequencies. As an example, dispersion curves of Rayleigh and Love waves at grid point (26°N, 102°E) are presented in Figure 2a. Finally, we use the neighborhood algorithm (NA) [*Sambridge*, 1999a, 1999b] to invert (for each grid-point) the dispersion data for variations of V_{SV} and V_{SH} with depth (Figure 2b); these 1-D profiles are combined into 3-D V_{SV} and V_{SH} models (Figure S2).

[8] The starting model for the 1-D inversion, after *Yao et al.* [2008], has an upper, middle, and lower crust, and the Moho depth is constrained by receiver function analysis [*Hu et al.*, 2005; *Xu et al.*, 2007]. To reduce the number of free parameters, V_P is scaled to V_{SV} using receiver function results [*Hu et al.*, 2005; *Xu et al.*, 2007], and ρ is related to V_P using empirical relations by *Brocher* [2005].

3. Shear Wave Velocity Structure and Radial Anisotropy

[9] The V_{SV} model obtained here from ambient noise interferometry agrees with the results that *Yao et al.* [2008] obtained from a combination of ambient noise interferometry and two-station analysis. In particular, LVZs are prominent in the middle and lower crust and some are bounded by faults, such as the Xianshuihe and Lijiang-Muli faults (Figure S2 of the auxiliary material).

[10] V_{SV} and V_{SH} are generally similar in the upper crust and upper mantle, but large differences occur in the middle and lower crust. A comparison of Love wave dispersion calculated from V_{SV} profiles (obtained from vertical component data) with the observed dispersion shows that these differences (and, hence, the implied radial anisotropy) are required by our data. For example, Figure 2a shows that for (25°N, 102°E) Love wave dispersion calculated from V_{SV} (cyan dashed line) is inconsistent with the observations (top red line with 1σ error bars), which are explained well by the V_{SH} model (black line).

[11] We quantify radial anisotropy, ψ, as $2(V_{SH} - V_{SV})/(V_{SH} + V_{SV})$*100%. In the upper crust ψ is less than 2% (Figure 3a), which we consider insignificant. In the middle and lower crust V_{SH} is generally larger than V_{SV} (Figures 3b, 3c, and 4), but strong anisotropy ($\psi > 5\%$) is detected in Songpan-Ganze block and in the southern part of our study region, between the Red River and the Xiaojiang fault. In the center of the study area a zone of relatively high V_{SV} ($\psi < 0$) is present in the middle and lower crust (Figures 3b, 3c, and 4). We note that uncertainty in the Moho depth only has a small

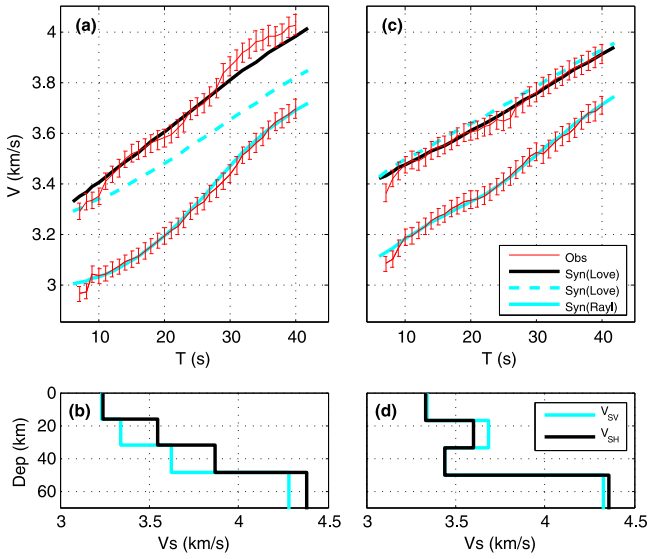

Figure 2. Rayleigh and Love phase velocity dispersion curves and shear wave speed models by the NA inversion at (a, b) (25°N, 102°E) and (c, d) (27.5°N, 102°E). In Figures 2a and 2c the red lines (with 1σ error bars) are observed phase velocity dispersion curves for Love (top) and Rayleigh (bottom) wave, respectively. The standard error σ is estimated from the seasonal variations of EGF [*Yao et al.*, 2006]. The black lines are the Love wave dispersion curves calculated from the V_{SH} model in Figures 2b and 2d, and the solid cyan lines are the calculated Rayleigh wave dispersion curve from the V_{SV} model in Figures 2b and 2d. The dashed cyan lines are the Love wave dispersion curve calculated from the V_{SV} model. In Figures 2(b) and 2(d) are V_{SH} (black) and V_{SV} (cyan) models obtained in NA inversion from the dispersion data shown in (a) and (c).

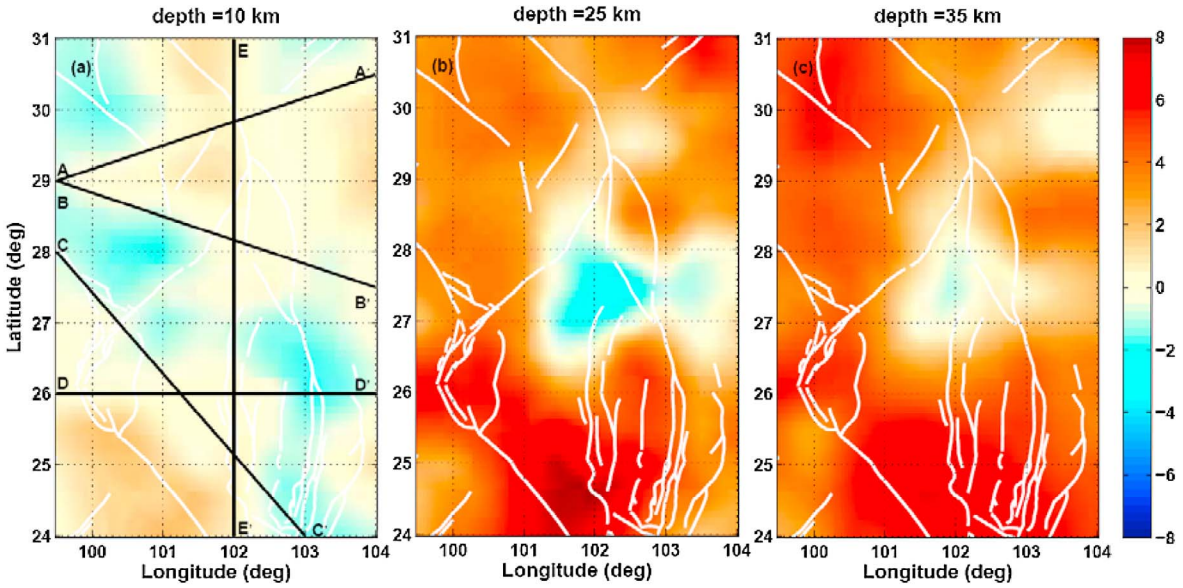

Figure 3. Radial anisotropy (ψ) defined as $2(V_{SH} - V_{SV})/(V_{SH} + V_{SV})$*100 (%), at (a) 10 km, (b) 25 km and (c) 35 km depth. Red depicts $V_{SH} > V_{SV}$ ($\psi > 0$); blue indicates $V_{SH} < V_{SV}$ ($\psi < 0$). White lines depict the major faults in our study area, and in Figure 3a the thin black lines with letters at each end indicate the location of vertical profiles in Figure 4.

effect on the estimate of radial anisotropy discussed here (see auxiliary material, Section 3).

4. Discussion and Conclusions

[12] GPS data [*Shen et al.*, 2005] suggest different surface velocities in areas bounded by the Xianshuihe-Xiaojiang, Litang, Lijiang-Muli, and Red River faults. Our current and previous studies reveal substantial crustal heterogeneity, and the tomographically observed contrasts across the Litang, Red River, and Xiaojiang faults at shallow depth (Figures S2a and S2d) and the Lijiang-Muli and Xianshuihe-Xiaojiang faults in the middle crust (Figures S2b and S2e) suggest that these faults are indeed major tectonic boundaries. Combined

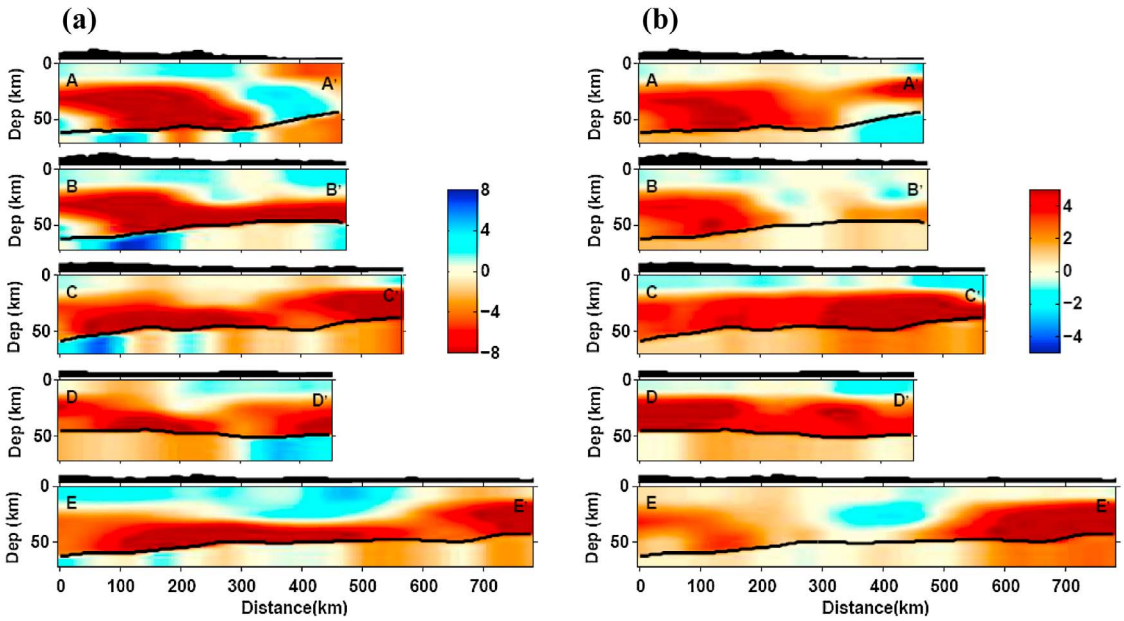

Figure 4. (a) The perturbation of shear wave velocity structure $d\ln V_{SV}$ (%), with red (blue) depicting slow (fast) shear wave propagation. Topography is shown above each profile. The black thick lines in each profile (around 50 km) depict the Moho discontinuity. The reference V_{SV} model in the curst is a 3 layered model with 3.3, 3.6, and 3.8 km/s in upper, middle and lower crust, which are inferred from the global Crust 2.0 model (http://mahi.ucsd.edu/Gabi/rem.html) by averaging Vs separately of the upper, middle, and lower crust for all locations with crustal thickness larger than 40 km. The reference V_{SV} in the upper mantle is the average of the whole study area. (b) Radial anisotropy, defined as $2(V_{SH} - V_{SV})/(V_{SH} + V_{SV})$*100 (%). Red represents $V_{SH} > V_{SV}$; and blue represents $V_{SH} < V_{SV}$.

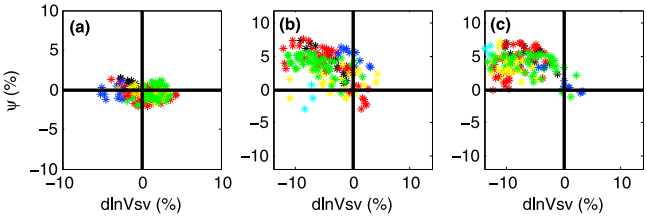

Figure 5. Relationship between relative V_{SV} anomalies (dlnV_{SV}) and radial anisotropy (ψ) for (a) upper crust, (b) middle crust, and (c) lower crust. Each symbol represents a grid point on map. Colors represent different tectonic regions (as defined in Figure S4): the Songpan-Ganze block (green), the Lhasa block (black), the Sichuan Basin (blue), the part of the Yangtze craton west of the Xianshuihe-Xiaojiang fault system (red), the part of the Yangtze block east of the Xianshuihe-Xiaojiang fault system (yellow), and the Youjiang block (cyan).

with other geophysical observables (e.g., heat flow, resistivity, Poisson's ratio) the anomalously low shear velocities indicate low (mechanical) rigidity [*Yao et al.*, 2008, 2010]. The ubiquitous LVZs may thus represent loci of ductile deformation in the deep crust. By themselves, however, they do not provide unequivocal evidence for horizontal flow.

[13] Our analysis of short-to-intermediate period horizontal and vertical component data suggests that, in general, radial anisotropy is weak at shallow depth but strong in the deep crust (with V_{SH} significantly larger than V_{SV}, that is, $\psi > 0$) (Figures 3 and 4). Interestingly, strong radial anisotropy occurs near the LVZs (that is, low V_{SV}) that were detected by *Yao et al.* [2008] and which are confirmed here. Indeed, in the middle crust of the Songpan-Ganze block and the part of the Yangtze craton between the Red River and Xiaojiang faults, V_{SV} is low and ψ is large ($V_{SH} > V_{SV}$). This is not always the case, however. Near the north end of the Luzhijiang fault, for instance, V_{SV} is relatively high and larger than V_{SH} ($\psi < 0$). We note that radial anisotropy here may not be significant since Love wave dispersion is, within error, consistent with the V_{SV} model (Figures 2c and 2d). The contrast with surrounding areas suggests that the small region confined by the Xianshuihe and Muli fault is relatively stable sub-block in the westernmost part of the Yangtze craton.

[14] For a more quantitative analysis of the relationship between wavespeed and radial anisotropy we plot radial anisotropy (ψ) versus shear velocity (dlnV_{SV}) for different tectonic regions and crust layers. In the upper crust (Figure 5a) radial anisotropy is small (less than 2%) and there is no correlation between V_{SV} and ψ. However, in the middle and lower crust, Figures 5b and 5c reveal a strong (negative) correlation between wavespeed and radial anisotropy in the lower crust beneath the western part of the study area (the Songpan-Ganze block, the westernmost part of the Yangtze craton and the Lhasa block) with LVZs (that is, dln$V_{SV} < 0$) coinciding with areas where $V_{SH} > V_{SV}$ (that is, $\psi > 0$). We also note that the LVZs themselves cannot simply be explained by radial anisotropy (see auxiliary material, Section 4, Figure S6).

[15] Radial anisotropy in the deep crust (with $V_{SH} > 0$) can be produced by a preferred orientation of mica crystals [*Weiss et al.*, 1999; *Nishizawa and Yoshitno*, 2001]. *Shapiro et al.* [2004] invoked a sub-horizontal mica fabric to explain radial anisotropy inferred from Love and Rayleigh wave propagation and to argue for thinning and lateral (channel) flow in the deep crust of Central Tibet. The strong radial anisotropy in and near LVZs inferred here may thus suggest (flow-induced) sub-horizontal alignment of mica in the mechanically weak zones of the deep crust beneath SE Tibet and SW China. This is consistent with deep crustal channel flow [e.g., *Royden et al.*, 1997], but lateral heterogeneity and the major faults in the region likely play an important role in controlling the pattern of such flow.

[16] **Acknowledgments.** We thank two anonymous reviewers for their constructive comments, which helped us improve the manuscript. We also thank the Editor Michael Wysession for his assistance. This work was supported by NSF grant EAR-0910618.

References

Bai, D., et al. (2010), Crustal deformation of the eastern Tibetan plateau revealed by magnetotelluric imaging, *Nat. Geosci.*, *3*, 358–362, doi:10.1038/ngeo830.

Brocher, T. M. (2005), Empirical relations between elastic wavespeeds and density in the Earth's crust, *Bull. Seismol. Soc. Am.*, *95*(6), 2081–2092, doi:10.1785/0120050077.

Hu, J., Y. Su, X. Zhu, and Y. Chen (2005), S-wave velocity and Poisson's ratio structure of crust in Yunnan and its implication (in Chinese), *Sci. China Ser. D*, *48*(2), 210–218, doi:10.1360/03yd0062.

Hu, S., L. He, and J. Wang (2000), Heat flow in the continental area of China: A new data set, *Earth Planet. Sci. Lett.*, *179*, 407–419, doi:10.1016/S0012-821X(00)00126-6.

Li, H., W. Su, C. Wang, and Z. Huang (2009), Ambient noise Rayleigh wave tomography in western Sichuan and eastern Tibet, *Earth Planet. Sci. Lett.*, *282*, 201–211, doi:10.1016/j.epsl.2009.03.021.

Lobkis, O. I., and R. L. Weaver (2001), On the emergence of the Green's function in the correlations of a diffuse field, *J. Acoust. Soc. Am.*, *110*(6), 3011–3017, doi:10.1121/1.1417528.

Moschetti, M. P., M. H. Ritzwoller, F. C. Lin, and Y. Yang (2010), Seismic evidence for widespread crustal deformation caused by extension in the western USA, *Nature*, *464*, 885–889, doi:10.1038/nature08951.

Nishizawa, O., and T. Yoshitno (2001), Seismic velocity anisotropy in mica-rich rocks: An inclusion model, *Geophys. J. Int.*, *145*, 19–32, doi:10.1111/j.1365-246X.2001.00331.x.

Roux, R., K. G. Sabra, W. A. Kuperman, and A. Roux (2005), Ambient noise cross correlation in free space: Theoretical approach, *J. Acoust. Soc. Am.*, *117*(1), 79–84, doi:10.1121/1.1830673.

Royden, L. H., B. C. Burchfiel, R. W. King, E. Wang, Z. Chen, F. Shen, and Y. Liu (1997), Surface deformation and lower crustal flow in eastern Tibet, *Science*, *276*, 788–790, doi:10.1126/science.276.5313.788.

Royden, L. H., B. C. Burchfiel, and R. D. van der Hilst (2008), The geological evolution of the Tibetan plateau, *Science*, *321*, 1054–1058, doi:10.1126/science.1155371.

Sambridge, M. (1999a), Geophysical inversion with a neighborhood algorithm—I. Searching a parameter space, *Geophys. J. Int.*, *138*(2), 479–494, doi:10.1046/j.1365-246X.1999.00876.x.

Sambridge, M. (1999b), Geophysical inversion with a neighborhood algorithm—II. Appraising the ensemble, *Geophys. J. Int.*, *138*(3), 727–746, doi:10.1046/j.1365-246x.1999.00900.x.

Shapiro, N. M., M. H. Ritzwoller, P. Molnar, and V. Levin (2004), Thinning and flow of Tibetan crust constrained by seismic anisotropy, *Science*, *305*, 233–236, doi:10.1126/science.1098276.

Shapiro, N. M., M. Campillo, L. Stehly, and M. H. Ritzwoller (2005), High-resolution surface-wave tomography from ambient seismic noise, *Science*, *307*, 1615–1618, doi:10.1126/science.1108339.

Shen, Z., J. Lv, M. Wang, and R. Burgmann (2005), Contemporary crustal deformation around the southeast borderland of the Tibetan Plateau, *J. Geophys. Res.*, *110*, B11409, doi:10.1029/2004JB003421.

Wang, E., and B. C. Burchfiel (2000), Late Cenozoic to Holocene deformation in southwestern Sichuan and adjacent Yunnan, China, and its role in formation of the southeastern part of the Tibetan Plateau, *Geol. Soc. Am. Bull.*, *112*, 413–423, doi:10.1130/0016-7606(2000)112<413:LCTHDI>2.0.CO;2.

Wang, E., et al. (Eds) (1999), *Late Cenozoic Xianshuihe-Xiaojiang, Red River, and Dali Fault Systems of Southwestern Sichuan and Central Yunnan, China*, *Spec. Pap. Geol. Soc. Am.*, 327, 114 pp.

Weaver, R., and O. I. Lobkis (2004), Diffuse fields in open systems and the emergence of the Green's function (L), *J. Acoust. Soc. Am.*, *116*(5), 2731–2734, doi:10.1121/1.1810232.

Weiss, T., S. Siegesmund, W. Rabbel, T. Bohlen, and M. Pohl (1999), Seismic velocities and anisotropy of the lower continental crust: A review, *Pure Appl. Geophys.*, *156*, 97–122, doi:10.1007/s000240050291.

Xu, L., S. Rondenay, and R. D. van der Hilst (2007), Structure of the crust beneath the southeastern Tibetan Plateau from teleseismic receiver functions, *Phys. Earth Planet. Inter.*, *165*, 176–193, doi:10.1016/j.pepi.2007.09.002.

Yao, H., R. D. Van der Hilst, and M. V. De Hoop (2006), Surface-wave array tomography in SE Tibet from ambient seismic noise and two-station analysis— I. Phase velocity maps, *Geophys. J. Int.*, *166*(2), 732–744, doi:10.1111/j.1365-246X.2006.03028.x.

Yao, H., C. Beghein, and R. D. Van der Hilst (2008), Surface wave array tomography in SE Tibet from ambient seismic noise and two-station analysis—II. Crustal- and upper-mantle structure, *Geophys. J. Int.*, *173*(1), 205–219, doi:10.1111/j.1365-246X.2007.03696.x.

Yao, H., R. D. Van der Hilst, and J. P. Montagner (2010), Heterogeneity and anisotropy of the lithosphere of SE Tibet from ambient noise and surface wave array tomography, *J. Geophys. Res.*, doi:10.1029/2009JB007142, in press.

Zhang, P., et al. (2004), Continuous deformation of the Tibetan Plateau from global positioning system data, *Geology*, *32*(9), 809–812, doi:10.1130/G20554.1.

H. Huang and R. D. van der Hilst, Department of Earth, Atmospheric, and Planetary Sciences, Massachusetts Institute of Technology, Cambridge, MA 02139, USA. (huanghui@mit.edu)

H. Yao, Institute of Geophysics and Planetary Physics, Scripps Institute of Oceanography, University of California, San Diego, La Jolla, CA 92093, USA.